Front. Mater. Sci. 2023, 17(3): 230655
https://doi.org/10.1007/s11706-023-0655-7

RESEARCH ARTICLE

Self-healing poly(acrylic acid) hydrogels fabricated by hydrogen bonding and Fe^{3+} ion cross-linking for cartilage tissue engineering

Min Kang[1], Yizhu Cheng[1], Yinchun Hu (✉)[1,2], Huixiu Ding[1], Hui Yang[1], Yan Wei[1,2], and Di Huang[1,2]

1 Research Center for Nano-Biomaterials & Regenerative Medicine, Department of Biomedical Engineering, College of Biomedical Engineering, Taiyuan University of Technology, Taiyuan 030024, China
2 Shanxi-Zheda Institute of Advanced Materials and Chemical Engineering, Taiyuan 030032, China

ABSTRACT: Autonomous self-healing hydrogels were achieved through a dynamic combination of hydrogen bonding and ferric ion (Fe^{3+}) migration. *N,N′*-methylenebis (acrylamide) (MBA), a cross-linking agent, was added in this study. Poly(acrylic acid) (PAA)/Fe^{3+} and PAA–MBA/Fe^{3+} hydrogels were prepared by introducing Fe^{3+} into the PAA hydrogel network. The ionic bonds were formed between Fe^{3+} ions and carboxyl groups. The microstructure, mechanical properties, and composition of hydrogels were characterized by field emission scanning electron microscopy and Fourier transform infrared spectroscopy. The experimental results showed that PAA/Fe^{3+} and PAA–MBA/Fe^{3+} hydrogels healed themselves without external stimuli. The PAA/Fe^{3+} hydrogel exhibited good mechanical properties, i.e., the tensile strength of 50 kPa, the breaking elongation of 750%, and the self-healing efficiency of 82%. Meanwhile, the PAA–MBA/Fe^{3+} hydrogel had a tensile strength of 120 kPa. These fabricated hydrogels are biocompatible, which may have promising applications in cartilage tissue engineering.

KEYWORDS: poly(acrylic acid); hydrogel; cartilage tissue; self-healing

Contents

Received May 24, 2023; accepted July 15, 2023

E-mail: huyinchun@tyut.edu.cn

1 Introduction

Articular cartilage is an essential tissue in the body's joints that provides support, cushioning, and lubrication. Its basic structure consists of the superficial, middle or transitional, deep or radial, and calcified cartilage zones [1–3]. As an essential structure in the human body, articular cartilage is susceptible to defects and damage due to impact and sprain during use [4–6]. The data show that cartilage damage and degeneration is a common orthopedic condition [7–10], and Widuchowski et al. [11] calculated 25124 arthroscopic knee procedures, up to 60% of cases were cartilage injuries. This is because articular cartilage has no blood vessels, no nerves, no immune response, and little ability to heal itself [12–14].

Because of their self-healing properties and resulting applications, these self-healing materials have attracted significant attention and are used to treat cartilage diseases [15–16]. Autonomous self-healing enables materials repair damage automatically and restore their normal properties, which as implants to replace damaged cartilage [17–18], while hydrogel is a soft material with a three-dimensional (3D) network structure and tunable physicochemical properties. Hydrogels are soft and flexible similar to extracellular matrix (ECM), and their 3D structure is also suitable for cell growth. Nowadays, hydrogels are widely used in biomedical fields such as wound dressing, drug delivery, and tissue engineering [19]. The application of self-healing hydrogels for repairing and replacing articular cartilage is currently a hot research topic due to their softness, viscoelasticity, and excellent biocompatibility [20–23]. Yu et al. combined the Diels–Alder click reaction with the acyl hydrazone bond to design and prepare a cross-linked double network (DN) hydrogel with a switch-on-off network structure with good self-healing and pH responsiveness [24]. Yang et al. prepared a polyvinyl alcohol (PVA) composite hydrogel containing polydopamine (PDA), which had ultra-fast near-infrared (NIR) light-triggered shape memory and self-healing capabilities [25]. Due to the excellent self-healing ability of PVA–PDA hydrogel, it has great potential in cartilage tissue engineering. Various self-healing hydrogels have been developed in the last few years using poly(ethylene glycol) methylether methacrylate (PEGMA) [26], PVA [27–28], poly(acrylamide) (PAM) [29–30], poly(acrylic acid) (PAA) [31], etc. In particular, PAA is a synthetic polymer consisting of acrylic acid (AA) monomer. It has been widely used in biomedical fields because of its excellent properties such as non-toxicity, high adhesive strength, and recyclability. At present, PAA has received great attention owing to its good self-healing properties deriving from high-content carboxyl groups that participate in the hydrogen bonding [32]. Peng et al. reported a reversible gel–sol/sol–gel transition in aqueous PAA solutions triggered by the redox state of iron ions and linked to photoreduction and oxidation [33]. Zhou et al. prepared PAA/cerium ions DN hydrogels and explored the self-healing properties of the hydrogels [31]. The hydrogel took about 12 h to complete its self-healing. Anjum et al. investigated the development of a highly absorbent PAA self-healing hydrogel using trivalent aluminum ions for ionic cross-linking [34]. PAA–Al hydrogels self-healed after 4 h, but the mechanical strength was low. Self-healing hydrogels usually have either high mechanical or rapid self-healing properties, but hardly both.

In this study, we reported a straightforward method to fabricate PAA/Fe^{3+} and PAA–*N*,*N*′-methylenebis (acrylamide) (MBA)/Fe^{3+} self-healing hydrogels without external stimuli or special conditions to achieve self-healing. The free radical polymerization of AA synthesized hydrogels in the presence of $FeCl_3$. The PAA chains polymerization produces chemically cross-linked to form a permanent hydrogel network. In contrast, the ionic bond between the Fe^{3+} and the carboxyl groups acts as a physical crosslink to form a secondary network within the hydrogel. Free Fe^{3+} ions move freely in the damaged region of the ionic cross-linked hydrogel, allowing the rapid recovery of broken chains. After the addition of MBA, the obtained hydrogels (named PAA–MBA/Fe^{3+} hydrogels) exhibited improved mechanical properties which varied with the MBA concentration. This work provides a simple method for the preparation of self-healing hydrogels and investigates their cytocompatibility, demonstrating their potential application in tissue engineering.

2 Materials and methods

2.1 Materials

PAA, $FeCl_3 \cdot 6H_2O$, MBA, and potassium persulfate (KPS) were purchased from Aladdin Reagent Co., Ltd. (Shanghai, China) and used as received. Millipore deionized water was used in all of the experiments. All other chemicals and solvents were of analytical grade.

2.2 Preparation of PAA/Fe^{3+} hydrogels

PAA/Fe^{3+} hydrogels were synthesized by radical polymerization and ionic cross-linking. In a typical procedure, KPS (1 wt.% of AA) was added to deionized water and the mixture was stirred. $FeCl_3 \cdot 6H_2O$ (0.5 mol.% of AA) and AA (20 wt.%) were added together to the above mixed homogenous aqueous solution. The solution was poured into a 120 mm × 120 mm × 1 mm mold with the bubbles removed and left at 45 °C for 6 h to form PAA/Fe^{3+} hydrogels.

2.3 Preparation of PAA–MBA/Fe^{3+} hydrogels

PAA–MBA/Fe^{3+} hydrogels were prepared from homogeneous aqueous solutions of KPS (1 wt.% AA), $FeCl_3 \cdot 6H_2O$ (0.5 mol.% AA), AA (20 wt.%), and different concentrations of MBA. The concentrations were 0.06 wt.% (MBA1), 0.08 wt.% (MBA2), 0.1 wt.% (MBA3), 0.5 wt.% (MBA4), 0.75 wt.% (MBA5), and 2.5 wt.% (MBA6). The rest preparation procedure was the same as that in Section 2.2.

2.4 Characterization

2.4.1 Scanning electron microscopy

PAA/Fe^{3+} and PAA–MBA/Fe^{3+} hydrogels were freeze-dried and quenched in liquid nitrogen to ensure the structural integrity of the fracture surface. All samples were covered with a layer of platinum (Pt). The morphology of the samples was investigated by scanning electron microscopy (SEM; JEOL JSM-7100F, Japan).

2.4.2 Fourier transform infrared spectroscopy

Samples were dried in a vacuum freeze dryer (−90 °C) for 24 h. The dried samples were mixed with potassium bromide at a mass ratio of 1:100 and ground to prepare slices. The infrared spectra of samples were measured from 4000 to 400 cm^{-1} by Fourier transform infrared spectroscopy (FTIR; Bruker Alpha, Germany) to distinguish the functional groups.

2.4.3 Water content and swelling ratio

The swollen PAA/Fe^{3+} and PAA–MBA/Fe^{3+} hydrogels were weighed after the surface water was wiped off with the filter paper, and then the hydrogels were vacuum-dried at 45 °C for 24 h. The water content (η) of the hydrogel was calculated by Eq. (1):

$$\eta/\% = \frac{m_{wet} - m_{dry}}{m_{wet}} \quad (1)$$

where m_{wet} and m_{dry} are masses of the swollen sample and the dried sample, respectively.

At 25 °C, the samples of known weight were immersed in the phosphate buffer solution (PBS). At certain time intervals, the samples were removed from the PBS and weighed after the excess water was wiped off from the sample surface with paper towels. Subsequently, they were put back into PBS immediately after weighing.

The swelling ratio (δ) was calculated according to Eq. (2):

$$\delta/\% = \frac{m_{wet} - m_{dry}}{m_{dry}} \quad (2)$$

where m_{wet} and m_{dry} are weights of the swollen gel and the initial dried gel, respectively.

2.4.4 Mechanical tests

Tensile tests and cyclic loading–unloading tests of the samples were characterized by a machine (REGER RGM-05, China) at room temperature. Dumbbell-shaped specimen strips with typical dimensions of 30 mm × 10 mm (length × width) were tested with a 50 N-load cell at the load speed of 100 $mm \cdot min^{-1}$. At least five specimens were tested for each sample to obtain the average value. The stress (σ_t) was measured based on following Eq. (3):

$$\sigma_t = \frac{F}{S} \quad (3)$$

where F is the maximum tensile load and S is the cross-sectional area of the hydrogel.

The strain (ε_t) was defined by following Eq. (4):

$$\varepsilon_t = \frac{\Delta L}{L_0} \tag{4}$$

where L_0 is the original length of the sample and ΔL is the length change relative to the gauge length of the free-standing specimen. Reliable results were obtained by averaging data from at least five specimens.

2.4.5 Cyclic loading–unloading test

The dumbbell-shaped sample was stretched at a strain rate of 100 mm·min^{-1} for the cyclic load–unload test. Two types of tests were performed with a 50 N-load cell:

(1) Continuous cyclic load–unloading test with increasing the maximum strain (100%, 200%, 300%, 400%, and 500%).

(2) Continuous cyclic loading–unloading test up to 300% strain for 10 cycles.

The cyclic continuous loading–unloading test was performed without waiting time. It was sufficient to stabilize the mechanical behavior in order to determine the resistance of the material to dynamic loading and check whether the material behaved similarly to the softening of natural tissues.

The hysteresis loop area, bounded by loading–unloading curves, indicated the dissipated energy or adsorbed energy per unit volume due to the viscous nature of the hydrogels and the water migration. The dissipation energy loss per unit volume (DEL; kJ·m^{-3}) during the hysteresis cycle was calculated from the area bounded within the hysteresis loop and defined as the following equation:

$$\mathrm{DEL} = \int_0^{\varepsilon_{max}} \sigma^+ \mathrm{d}\varepsilon + \int_{\varepsilon_{max}}^0 \sigma^- \mathrm{d}\varepsilon \tag{5}$$

2.5 Self-healing tests of hydrogels

To test self-healing properties, the hydrogel was cut into two pieces. One piece was stained with methyl blue (MB) dye, and the cracks were aligned with each other for self-healing testing at room temperature. The self-healing effect was judged by observing the state of the cracks. The tensile tests of the healed hydrogels were performed as described in Section 2.4.4.

The healing efficiency (HE) is defined by the following equation:

$$\mathrm{HE}/\% = \frac{L_h}{L_o} \tag{6}$$

where L_h and L_o are tensile lengths of the healed sample and the original sample, respectively. The mean and error were calculated from at least five independent specimens of each sample.

2.6 Cytocompatibility studies

2.6.1 Chondrocyte isolation and culture

Chondrocytes were isolated from rat articular cartilage, briefly, blocks of cartilage were cut into small pieces (1 mm^3) and digested with 0.25% trypsin for 0.5 h, followed by 0.1% type II collagenase for 6 h. The released cells were collected and cultured in the presence of 10% fetal bovine serum (FBS), 100 U·mL^{-1} penicillin, and 100 g·mL^{-1} streptomycin in Dulbecco's modified Eagle's medium (DMEM). To preserve the chondrocyte phenotype, chondrocytes within three generations were used [35].

2.6.2 Cell culture

The samples were cut into discs by using a puncher and placed in the 48-well plate. All samples were sterilized three times with alcohol for 5 min each time and sterilized by ultraviolet irradiation overnight. After sterilization, the hydrogels were immersed in DMEM overnight. A cell suspension was added to each well at a density of 1.0×10^4 cells/well for the cytotoxicity test, cell proliferation test, and cytoskeleton staining. All plates were placed in an incubator with the humidified atmosphere of 5% CO_2 at 37 °C. The cell culture medium (DMEM containing 10% FBS and 1% penicillin/streptomycin) was changed every 2 d.

2.6.3 Cell proliferation test

The Cell Counting Kit-8 (CCK-8) is widely used for rapid and highly sensitive detection of cell proliferation and cytotoxicity. After the addition of the CCK-8 solution, the more cells proliferate, the darker the color; the more cytotoxic, the lighter the color. For the same cell, the intensity of the color is linearly related to the number of cells. The medium was removed at a specific time point, and each well was washed three times with PBS. The cell culture medium containing 10% CCK-8 solution was

added to each well and incubated in a cell incubator for 3 h. After incubation, 200 μL mixed solution was used to measure the absorbance at 450 nm.

2.6.4 Cytoskeleton staining

Hoechst 33258 (Beyotime, China) was used for nuclear staining, and Actin-Tracker Green-488 (Beyotime, China) was used for actin microfilament staining. The actin staining working solution was prepared according to the kit instruction. After the samples and chondrocyte cells were co-cultured for 1, 3, and 5 d, the culture solution was removed. Each well was washed three times with PBS. The 4% formaldehyde solution was used to fix the cells for 15 min at room temperature. After washing three times with PBS containing 0.1% Triton X-100, 100 μL actin staining working solution was added into each well and incubated for 40 min in the dark. After incubation, 100 μL Hoechst staining solution was added into each well at room temperature for 10 min. After washing, a fluorescent inverted microscope was used to observe the cytoskeleton morphology.

2.7 Statistical analysis

All data were expressed as means ± standard deviations (SD) and were analyzed using one-way analysis of variance (ANOVA). A P value less than 0.05 was considered to be statistically significant ($*P < 0.05$, $**P < 0.01$, $***P < 0.001$).

3 Results and discussion

3.1 Morphology characteristics

The morphology of PAA/Fe^{3+} and $PAA–MBA/Fe^{3+}$ hydrogels was observed by SEM. The porous structure appeared in PAA/Fe^{3+} hydrogels (Figs. 1(a) and 1(b)) and $PAA–MBA/Fe^{3+}$ hydrogels (Figs. 1(c) and 1(d)). PAA/Fe^{3+} hydrogels had a homogeneous pore structure, and $PAA–MBA/Fe^{3+}$ hydrogels had a changed structure with denser pores compared to PAA/Fe^{3+} hydrogels, which might be due to the addition of MBA to improve the cross-linking degree of the hydrogels. The structure of the hydrogel might be related to its strength and tensile properties.

FTIR spectra of the PAA/Fe^{3+} hydrogel and

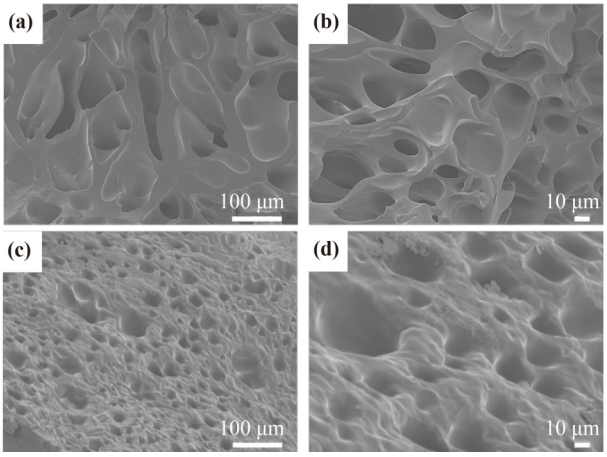

Fig. 1 The morphology and microstructure of (**a**)(**b**) PAA/Fe^{3+} and (**c**)(**d**) $PAA–MBA/Fe^{3+}$.

$PAA–MBA/Fe^{3+}$ hydrogels with different MBA contents are shown in Fig. 2. The characteristic peak near 1450 cm^{-1} shown by the FTIR spectrum corresponds to the C−O bond from the carboxyl group, and a broad absorption peak of 3447 cm^{-1} is the absorption of hydroxyl groups (−OH) in PAA. The stretching vibration peak of the Fe−O bond at 610 cm^{-1} is observed in the FTIR analysis suggesting the ionic cross-linking between carboxyl groups of PAA and Fe^{3+}. The significant change at 1540 cm^{-1} could indicate that the MBA and PAA chains are cross-linked, which is the characteristic peak of the N−H bond in MBA.

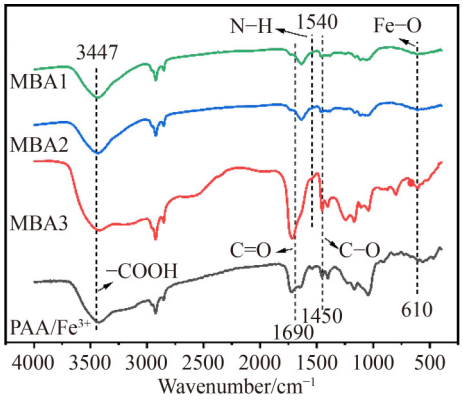

Fig. 2 FTIR spectra of PAA/Fe^{3+} hydrogel and $PAA–MBA/Fe^{3+}$ hydrogel with different MBA contents.

3.2 Water content and swelling ratio

The hydrogel is a material with high water content. As shown in Fig. 3(a), the water contents were (77.73±3.3)% for the PAA hydrogel, (72.02±8.7)% for the PAA/Fe^{3+}

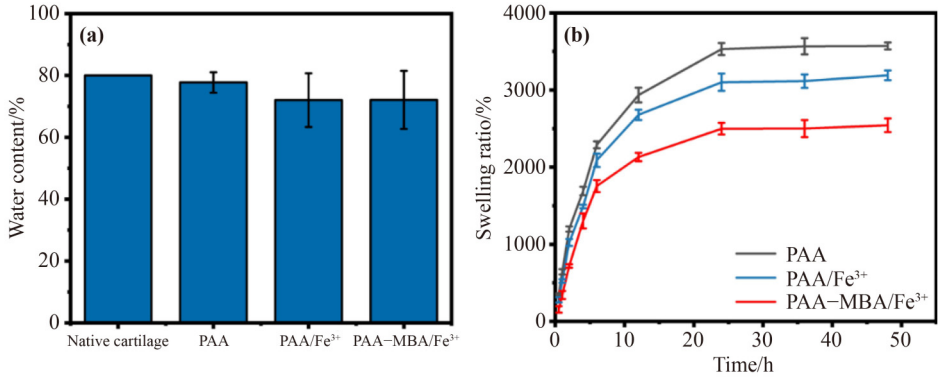

Fig. 3 (**a**) Water contents and (**b**) swelling ratios of PAA hydrogel, PAA/Fe^{3+} hydrogel, and PAA–MBA/Fe^{3+} hydrogel.

hydrogel, while (72.11±9.4)% for the PAA–MBA/Fe^{3+} hydrogel. Figure 3(a) showed that the difference in water content among the three hydrogels was not significant when Fe^{3+} and MBA were added, which indicated that the addition of Fe^{3+} and MBA does not affect hydrophilic properties of the PAA hydrogel, and all of them were similar to the water content of natural cartilage in humans. As seen in Fig. 3(b), PAA had an extremely high swelling rate, while the swelling rate decreased after the addition of Fe^{3+}, which was due to the interaction between polymer chains caused by the ionic cross-linking, resulting in the enhanced hydrophobic linkage between hydrogel chains. And the swelling ratio of PAA–MBA/Fe^{3+} hydrogel further decreased after the addition of MBA, which was due to the formation of the chemical cross-linked network limiting the structure of the hydrogel.

3.3 Mechanical properties of hydrogels

To evaluate the influence of the MBA content on mechanical properties of hydrogels, the mechanical behaviors of PAA/Fe^{3+} and PAA–MBA/Fe^{3+} hydrogels were characterized by tensile tests. The results for PAA/Fe^{3+} hydrogels and PAA–MBA/Fe^{3+} hydrogels with different MBA contents are shown in Fig. 4.

As shown in Fig. 4(a), with increasing the MBA concentration, the stresses and strains in the hydrogel show a trend of increasing and then decreasing. The PAA/Fe^{3+} hydrogel shows the stress below 50 kPa and the Young's modulus below 20 kPa in Figs. 4(b) and 4(c). This is because the AA contains intermolecular hydrogen bonds internally to form a first cross-linked network, after which COO^- groups on the PAA chains and Fe^{3+} ligand complexes form coordination bonds to build a second cross-linked network, in which hydrogen and ionic bonds together provide energy dissipation to the hydrogel. The mechanical properties of the hydrogel increased as the MBA was added when the content of MBA was increased to 0.1 wt.%, the tensile stress of PAA–MBA/Fe^{3+} hydrogel increased from 50 to 118 kPa in Fig. 4(b), the breaking elongation increased from 697% to 855% in Fig. 4(d), and the tensile modulus decreased from 26 to 21 kPa in Fig. 4(c). This is because MBA has two active reactive functional groups that swiftly and rapidly transform the polymer from a linear structure to a 3D network structure, which is chemically cross-linked with PAA molecular chains to form a cross-linked network. It is also consistent with the microscopic image in Fig. 1.

However, as shown in Fig. 4(a), the concentration of MBA is too high, which, on the contrary, significantly affects the hydrogel itself, not only is in terms of tensile strength, but also causes a precipitous drop in its breaking elongation, which is not in line with the purpose of this research. This is caused by excessive cross-linking, and the crystal structure has changed, or even lost the original crystal lattice structure, causing the molecular chain to break, thus reducing tensile strength and breaking elongation.

In conclusion, the addition of MBA effectively enhances the mechanical properties of the PAA/Fe^{3+} hydrogel, and the hydrogel reaches the maximum tensile stress and breaking elongation when the MBA concentration is 0.1 wt.%. And as shown in Fig. 4, the high concentration of the MBA, on the contrary, may lead to a decrease in the hydrogel strength, so 0.6, 0.8, and 0.1 wt.% are chosen for further study.

3.4 Cyclic loading–unloading properties

With the enhancement of the dissipation energy, the

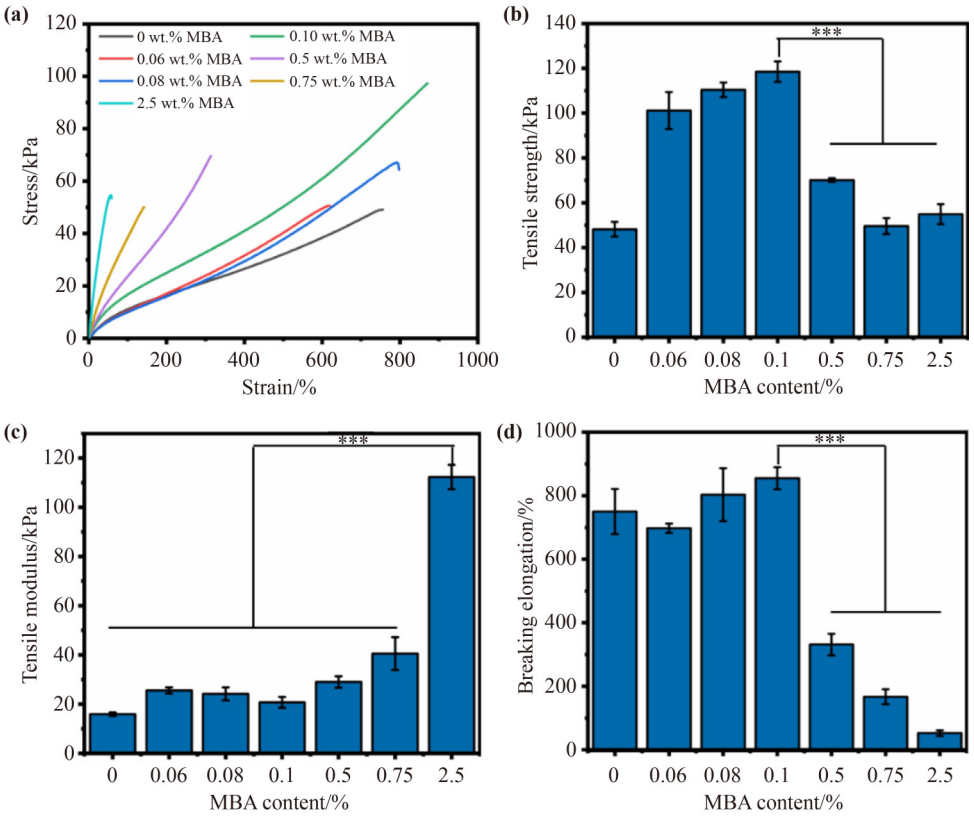

Fig. 4 (**a**) Tensile stress–strain curves of PAA–MBA/Fe^{3+} hydrogels with different contents of MBA. (**b**) Tensile strength, (**c**) tensile modulus, and (**d**) breaking elongation values corresponding to different contents of MBA.

strength of hydrogels improves. The cyclic loading–unloading tests were carried out to study the fatigue resistance of PAA/Fe^{3+} and PAA–MBA3/Fe^{3+} hydrogels (Fig. 5). Firstly, the hydrogel was cyclically stretched at 100%, 200%, 300%, 400%, and 500% strains separately, and the stress–strain curves are shown in Figs. 5(a) and 5(b), while the dissipated energy comparison results are shown in Fig. 5(c). It was seen that the addition of MBA could effectively increase the dissipation energy of the hydrogel at the same tensile strain, meaning that the hydrogel with the addition of MBA better disperses the stress without destroying its internal structure at the same stress, which is the reason for its better mechanical properties. The addition of MBA transformed the hydrogel into a 3D network structure and led to the formation of chemical cross-linked bonds allowed for better stress dispersion so that PAA–MBA/Fe^{3+} hydrogel had higher dissipation energy.

Then, the samples were subjected to a 300% strain loading–unloading test with 10 cycles of 30 s between each to test the fatigue resistance of the hydrogel over a short period. The stress–strain curves are shown in Figs. 5(d) and 5(e), and the dissipation energy comparison results are shown in Fig. 5(f). It could be seen that at the same strain of 10 cycles of stretching, the PAA–MBA/Fe^{3+} hydrogel has higher mechanical strength and finally reaches 40% of the initial state, which is superior to that of the PAA/Fe^{3+} hydrogel, indicating that the PAA–MBA/Fe^{3+} hydrogel is more adaptable to frequent stretching activities and has better anti-fatigue performance.

In general, the 3D network structure of the hydrogel formed by the addition of MBA effectively dissipates the energy during the stretching process, which gives the hydrogel its outstanding mechanical properties.

3.5 Self-healing properties

The hydrogel performs self-healing properties based on the dynamic and reversible nature of hydrophobic association and ionic bonding of polymer chains, and the reaction mechanism is shown in Fig. 6. The self-healing of hydrogels is motivated by dynamic ionic bonding between Fe^{3+} ions and carboxyl groups of PAA. Multiple ionic interactions between Fe^{3+} ions and carboxyl groups

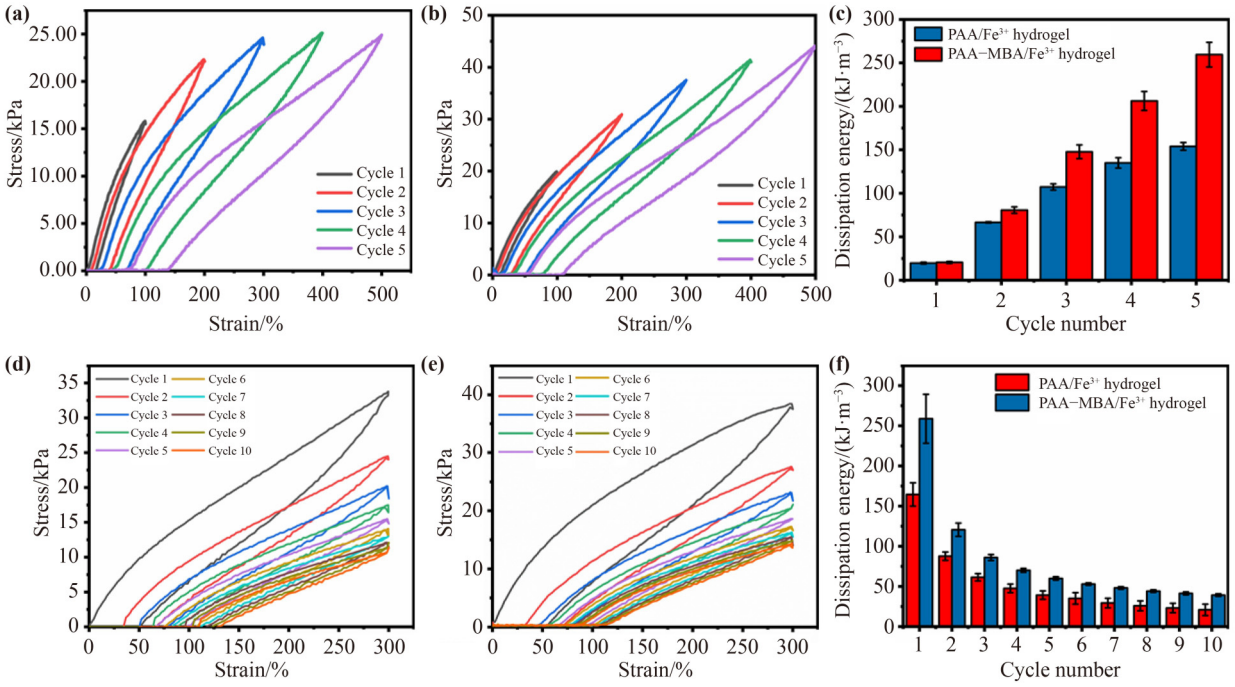

Fig. 5 Cyclic stress–strain curves at different strains of (**a**) PAA/Fe^{3+} hydrogel and (**b**) PAA–MBA3/Fe^{3+} hydrogel. (**c**) Dissipated energy of PAA/Fe^{3+} hydrogel and PAA–MBA3/Fe^{3+} hydrogel at different strains. Cyclic stress–strain curves at 300% strain of (**d**) PAA/Fe^{3+} hydrogel and (**e**) PAA–MBA3/Fe^{3+} hydrogel. (**f**) Dissipated energy of PAA/Fe^{3+} hydrogel and PAA–MBA3/Fe^{3+} hydrogel at 300% strain.

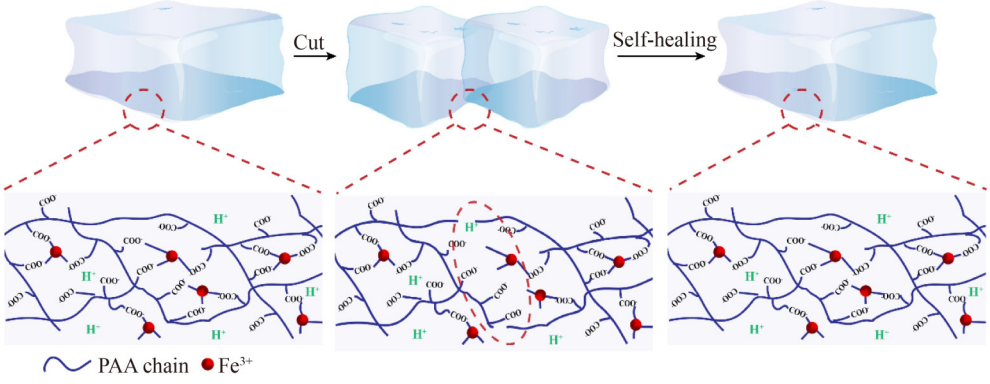

Fig. 6 Self-healing mechanism of the PAA/Fe^{3+} hydrogel.

of PAA produce a non-covalent network of polymer chains. The dynamic nature of ionic interactions plays a crucial role in self-healing. Iron ions diffuse towards the newly cut interface and interact with carboxyl groups of PAA chains with the help of the mobility of PAA chain segments. The binding between PAA and Fe^{3+} ions at the interface between chains repairs the damage and reconnects the two gel pieces. Since the self-healing process only alters the non-covalent network, it impairs the mechanical strength of the hydrogel.

To test the self-healing performance of the PAA/Fe^{3+} hydrogel, as shown in Fig. 7(a), the hydrogel was cut into two pieces, one of which was stained with the MB dye, and the two sections were aligned to keep them in contact with each other, placed at room temperature waiting for the occurrence of its self-healing. After 30 min, the cracks were visible to heal, and 5 h later, the self-healing of the PAA/Fe^{3+} hydrogel was completed, the hydrogel stretched without fracture, and the cracks completely disappeared under the microscope as shown in Fig. 7(b). Figure 7(c) shows the comparison of the original and healed hydrogels. After 5 h, the stress of the healed gel could reach 81.5% of the original sample. A comparison of tensile strength, modulus of elasticity, and breaking

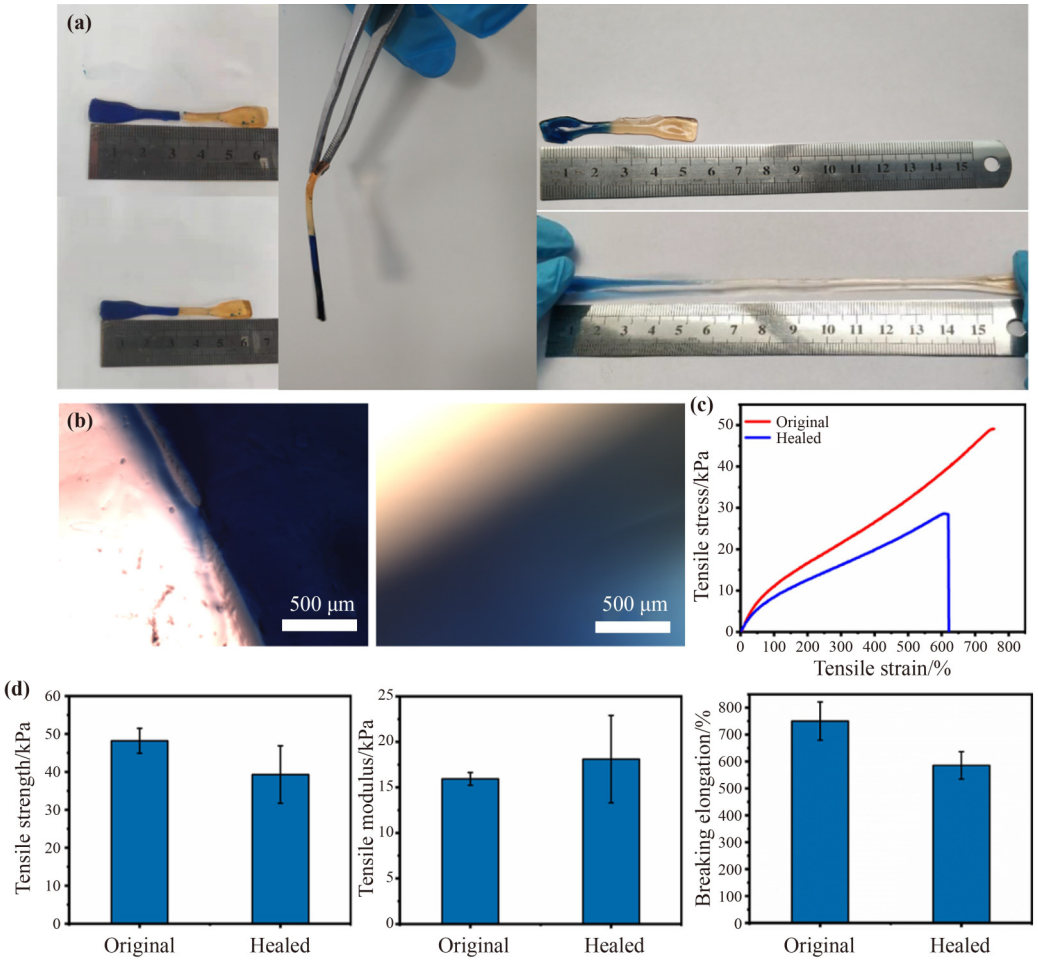

Fig. 7 (**a**) Mechanical stretching of the healed PAA/Fe^{3+} hydrogel. (**b**) Optical microscopy images of fresh cut on PAA/Fe^{3+} hydrogel and complete self-healed cracks after 5 h. (**c**)(**d**) The self-healing properties of the PAA/Fe^{3+} hydrogel.

elongation before and after self-healing was also obtained (Fig. 7(d)). The self-repaired hydrogels showed a decrease in tensile strength and breaking elongation, while the tensile modulus increased. It suggests that the PAA/Fe^{3+} hydrogel has excellent self-healing properties.

To investigate the effect of MBA on the self-healing properties of PAA/Fe^{3+} hydrogels, self-healing tests were performed on PAA–MBA/Fe^{3+} hydrogels at 0.6, 0.8, and 0.1 wt.% concentrations considering the results in Section 3.4. The healing rate became significantly slower and did not heal completely after 5 h. The hydrogel healed completely after only 24 h (Fig. 8(a)). A comparison of stress–strain curves of the original and healed hydrogels is shown in Fig. 7(b), and HE values are shown in Fig. 8(c). Compared with that of the PAA/Fe^{3+} hydrogel, the self-healing efficiency of PAA–MBA/Fe^{3+} hydrogels was significantly lower, and the HE of healed gels reached 50% of the original samples. This is because the MBA is chemically cross-linked with the PAA, and the chemical covalent bonds formed cannot be re-formed once they were broken.

3.6 *In vitro* biological evaluation

Biocompatibility is an important property of biomaterials. PAA hydrogel, PAA/Fe^{3+} hydrogel, and PAA–MBA3/Fe^{3+} hydrogel were chosen for the relevant experiments. After 1, 3, and 5 d of culture, cell proliferation was measured for each group using CCK-8. The cell proliferation of different hydrogels is shown in Fig. 9(a). The optical density (OD) values of all hydrogels increased with the rise of the incubation time, indicating that all the four groups of samples were non-toxic, and the addition of Fe^{3+} and MBA did not affect the cytocompatibility of PAA. All hydrogel groups had good cytocompatibility.

The spreading of cells is also a comprehensive reflection of the cytoskeleton assembly and closely related

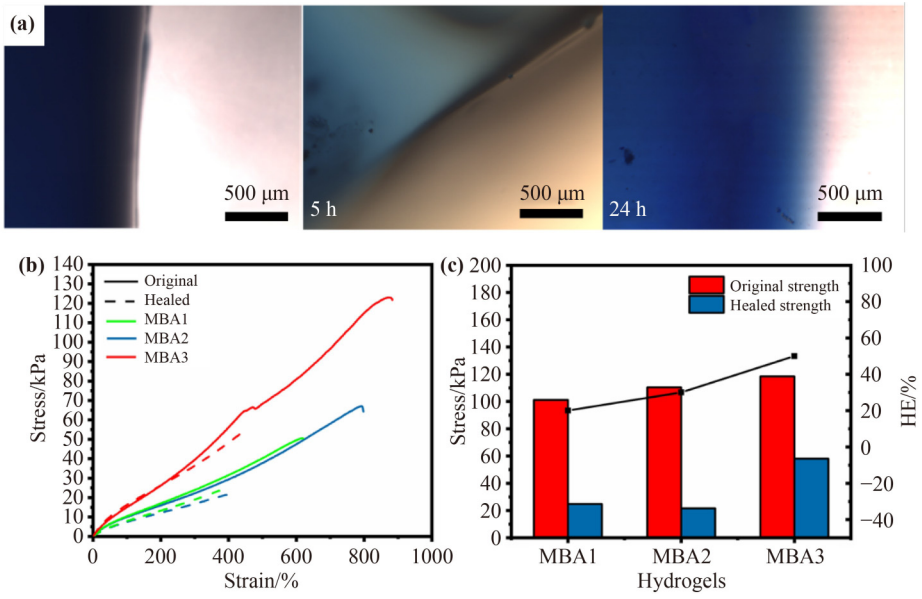

Fig. 8 (**a**) Optical microscopy images of the self-healing process in PAA–MBA/Fe^{3+} hydrogels at 0 min, 5 h later, and 24 h later. (**b**) Tensile strain–stress curves of healed PAA–MBA/Fe^{3+} hydrogels with different MBA contents. (**c**) Tensile strengths and HE values of original and self-healed hydrogels with different MBA contents.

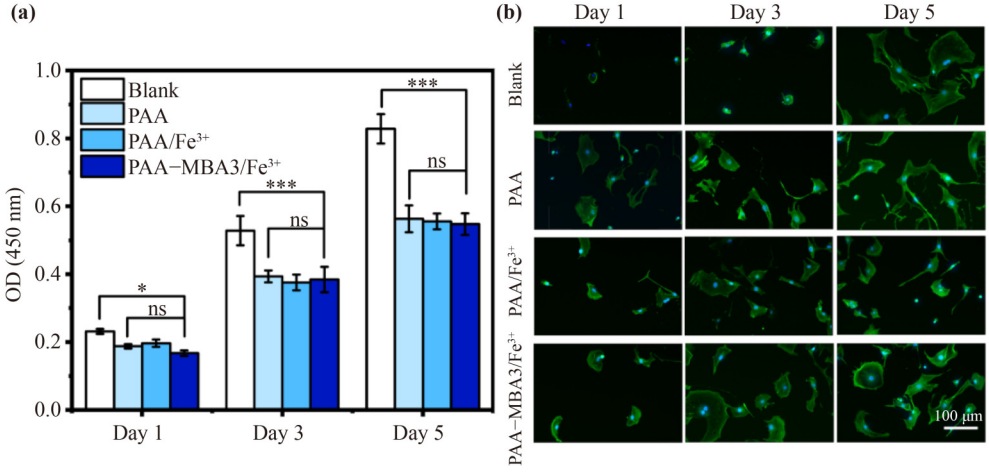

Fig. 9 (**a**) Proliferation analysis on the surface of different samples assessed by the CCK-8 method. (**b**) Actin filament staining of chondrocytes on the hydrogels after culturing for 1, 3, and 5 d.

to the growth of cells [36–37]. After staining with fluorescein isothiocyanate (FITC)-labeled phalloidin and Hoest reagent, the adhesion and morphology of chondrocytes on the hydrogel surface can be clearly observed. Figure 9(b) shows the cytoskeletal organization, attachment, and spreading of cells cultured on PAA hydrogel, PAA/Fe^{3+} hydrogel, and PAA–MBA3/Fe^{3+} hydrogel for 1, 3, and 5 d. It is seen that round or oval nuclei were stained in blue, while cytoskeletons composed of microfilaments were stained in green. There is no significant difference in cell morphology between hydrogel surfaces, with cells fully extended and pseudopods attached to the hydrogel surface or to adjacent cells. The results suggest that PAA/Fe^{3+} hydrogels and PAA–MBA/Fe^{3+} hydrogels exhibit characteristics of biocompatibility with good cell adhesion.

4 Conclusions

In summary, PAA/Fe^{3+} hydrogels and PAA–MBA/Fe^{3+} hydrogels were prepared in this study, both of which revealed good mechanical properties. Synthetic PAA/Fe^{3+} hydrogels and PAA–MBA/Fe^{3+} hydrogels showed

autonomous and effective healing property without any external intervention. The PAA/Fe^{3+} ionic cross-linked hydrogel had good self-healing efficiency (82%), with a healing time of 5 h at room temperature, whereas the PAA–MBA/Fe^{3+} hydrogel completed self-healing at room temperature for 24 h, reducing the HE to 50%. It was revealed by the cyclic loading–unloading test that the hydrogel had enhanced dissipation energy after the addition of MBA as well as had better fatigue resistance. Meanwhile, biocompatibility tests demonstrated that both of the hydrogels were biocompatible. Therefore, it is believed that PAA/Fe^{3+} hydrogels offer attractive prospects and can be extended to further applications in tissue engineering, sensors, and drug carriers due to their high performance, self-healing, and bio-friendly properties.

Disclosure of potential conflicts of interests No potential conflict of interest was reported by the authors.

Acknowledgements This work was supported by the General Project of Natural Science of Shanxi Provincial Basic Research Program (Grant No. 202203021211125) and the National Natural Science Foundation of China (Grant No. 11802197).

References

[1] Francis Suh J K, Matthew H W T. Application of chitosan-based polysaccharide biomaterials in cartilage tissue engineering: a review. Biomaterials, 2000, 21(24): 2589–2598

[2] Martel-Pelletier J, Boileau C, Pelletier J P, et al. Cartilage in normal and osteoarthritis conditions. Best Practice & Research. Clinical Rheumatology, 2008, 22(2): 351–384

[3] Hunter W. Of the structure and disease of articulating cartilages. 1743. Clinical Orthopaedics and Related Research, 1995, (317): 3–6

[4] Buckwalter J A, Lane N E. Athletics and osteoarthritis. The American Journal of Sports Medicine, 1997, 25(6): 873–881

[5] Martin J A, Buckwalter J A. Roles of articular cartilage aging and chondrocyte senescence in the pathogenesis of osteoarthritis. The Iowa Orthopaedic Journal, 2001, 21: 1–7

[6] Martin J A, Buckwalter J A. Aging, articular cartilage chondrocyte senescence and osteoarthritis. Biogerontology, 2002, 3(5): 257–264

[7] de Windt T S, Vonk L A, Brittberg M, et al. Treatment and prevention of (early) osteoarthritis using articular cartilage repair — fact or fiction? A systematic review Cartilage, 2013, 4(3 Suppl): 5S–12S

[8] Chang C-H, Lin F-H, Kuo T-F, et al. Cartilage tissue engineering. Biomedical Engineering: Applications, Basis and Communications, 2005, 17(2): 61–71

[9] Solchaga L A, Goldberg V M, Caplan A I. Cartilage regeneration using principles of tissue engineering. Clinical Orthopaedics and Related Research, 2001, 391(Suppl): S161–S170

[10] Buckwalter J A, Mankin H J. Articular cartilage: degeneration and osteoarthritis, repair, regeneration, and transplantation. Instructional Course Lectures, 1998, 47: 487–504

[11] Widuchowski W, Widuchowski J, Trzaska T. Articular cartilage defects: study of 25,124 knee arthroscopies. Knee, 2007, 14(3): 177–182

[12] Athanasiou K A, Shah A R, Hernandez R J, et al. Basic science of articular cartilage repair. Clinics in Sports Medicine, 2001, 20(2): 223–247

[13] Hayes D W Jr, Brower R L, John K J. Articular cartilage. Anatomy, injury, and repair. Clinics in Podiatric Medicine and Surgery, 2001, 18(1): 35–53

[14] Hunziker E B. Articular cartilage repair: basic science and clinical progress. A review of the current status and prospects. Osteoarthritis and Cartilage, 2002, 10(6): 432–463

[15] Zheng Q, Ma Z, Gong S. Multi-stimuli-responsive self-healing metallo–supramolecular polymer nanocomposites. Journal of Materials Chemistry A: Materials for Energy and Sustainability, 2016, 4(9): 3324–3334

[16] Song M M, Wang Y M, Liang X Y, et al. Functional materials with self-healing properties: a review. Soft Matter, 2019, 15(33): 6615–6625

[17] Beddoes C M, Whitehouse M R, Briscoe W H, et al. Hydrogels as a replacement material for damaged articular hyaline cartilage. Materials, 2016, 9(6): 443

[18] Li L, Yu F, Zheng L, et al. Natural hydrogels for cartilage regeneration: modification, preparation and application. Journal of Orthopaedic Translation, 2019, 17: 26–41

[19] Liu J, Qu S, Suo Z, et al. Functional hydrogel coatings. National Science Review, 2021, 8(2): nwaa254

[20] Calvert P. Hydrogels for soft machines. Advanced Materials, 2009, 21(7): 743–756

[21] Taylor D L, Panhuis M I H. Self-healing hydrogels. Advanced Materials, 2016, 28(41): 9060–9093

[22] Hillewaere X K D, Du Prez F E. Fifteen chemistries for autonomous external self-healing polymers and composites. Progress in Polymer Science, 2015, 49–50: 121–153

[23] Bakarich S E, Gorkin R, Panhuis M I H, et al. Three-dimensional printing fiber reinforced hydrogel composites. ACS Applied Materials & Interfaces, 2014, 6(18): 15998–16006

[24] Yu F, Cao X, Du J, et al. Multifunctional hydrogel with good structure integrity, self-healing, and tissue-adhesive property

formed by combining die is alder click reaction and acylhydrazone bond. ACS Applied Materials & Interfaces, 2015, 7(43): 24023–24031

[25] Yang L, Wang Z, Fei G, et al. Polydopamine particles reinforced poly(vinyl alcohol) hydrogel with NIR light triggered shape memory and self-healing capability. Macromolecular Rapid Communications, 2017, 38(23): 1700421

[26] Yang W J, Tao X, Zhao T, et al. Antifouling and antibacterial hydrogel coatings with self-healing properties based on a dynamic disulfide exchange reaction. Polymer Chemistry, 2015, 6(39): 7027–7035

[27] Tie J, Liu H, Lv J, et al. Multi-responsive, self-healing and adhesive PVA based hydrogels induced by the ultrafast complexation of Fe^{3+} ions. Soft Matter, 2019, 15(37): 7404–7411

[28] Zhang H, Xia H, Zhao Y. Poly(vinyl alcohol) hydrogel can autonomously self-heal. ACS Macro Letters, 2012, 1(11): 1233–1236

[29] Okay O. In: Seiffert S, ed. Supramolecular Polymer Networks and Gels. Springer, 2015

[30] Deng Y, Huang M, Sun D, et al. Dual physically cross-linked κ-carrageenan-based double network hydrogels with superior self-healing performance for biomedical application. ACS Applied Materials & Interfaces, 2018, 10(43): 37544–37554

[31] Zhou H, Xu G, Li J, et al. Preparation and self-healing behaviors of poly(acrylic acid)/cerium ions double network hydrogels. Macromolecular Research, 2015, 23(12): 1098–1102

[32] Dalei G, Das S. Polyacrylic acid-based drug delivery systems: a comprehensive review on the state-of-art. Journal of Drug Delivery Science and Technology, 2022, 78: 103988

[33] Peng F, Li G, Liu X, et al. Redox-responsive gel–sol/sol–gel transition in poly(acrylic acid) aqueous solution containing Fe(III) ions switched by light. Journal of the American Chemical Society, 2008, 130(48): 16166–16167

[34] Anjum S, Gurave P, Badiger M V, et al. Design and development of trivalent aluminum ions induced self healing polyacrylic acid novel hydrogels. Polymer, 2017, 126: 196–205

[35] Gosset M, Berenbaum F, Thirion S, et al. Primary culture and phenotyping of murine chondrocytes. Nature Protocols, 2008, 3(8): 1253–1260

[36] Gumbiner B M. Cell adhesion: the molecular basis of tissue architecture and morphogenesis. Cell, 1996, 84(3): 345–357

[37] Parker K K, Brock A L, Brangwynne C, et al. Directional control of lamellipodia extension by constraining cell shape and orienting cell tractional forces. FASEB Journal, 2002, 16(10): 1195–1204